

The Time-of-Flight Technique for the HERMES Experiment

A. Airapetian^e, N. Akopov^e, M. Amarian^{d,e}, H. Avakian^{b,e},
A. Avetissian^e, E. Avetisyan^{b,e}, B.W. Filippone^a, R. Kaiser^c,
H. Zohrabian^e,

^a*W.K. Kellogg Radiation Lab, California Institute of Technology,
Pasadena, California 91125, USA*

^b*INFN, Laboratori Nazionali di Frascati, 00044 Frascati, Italy*

^c*University of Glasgow, Dept. of Physics and Astronomy,
Glasgow G12 8QQ, Scotland, U.K.*

^d*INFN, Sezione Sanita, 00161 Roma, Italy*

^e*Yerevan Physics Institute, 375036 Yerevan, Armenia*

arXiv:hep-ex/0301010v3 16 Nov 2004

Abstract

This paper describes the use of the time-of-flight (TOF) technique as a particle identification method for the HERMES experiment. The time-of-flight is measured by two $1 \times 4m^2$ scintillation hodoscopes that initially were designed for the first-level trigger only. However, the suitable time structure of the HERA electron beam allows an extension of their functions to also measure the TOF for low momentum hadron identification. Using only these conventional hodoscopes, good particle identification was achieved for protons and pions in the momentum range up to 2.9 GeV/c and for kaons up to 1.5 GeV/c.

PACS number 29.30.-h, 29.40.-n, 29.40.Gx, 29.40.Mc

Keywords: particle identification, time-of-flight

1 Introduction

The HERMES experiment at DESY [1] is a second generation polarised deep-inelastic scattering experiment to study the spin structure of the nucleon. Several experiments over the last decade have provided accurate data on the polarisation asymmetry of the cross-section for *inclusive* scattering where only the scattered lepton is detected. Further knowledge of the origin of the nucleon's spin can be gained by studying *semi-inclusive* processes involving the detection of hadrons in coincidence with the scattered lepton. This increases the demands on hadron identification of the detection system.

The time-of-flight (TOF) particle identification method is a fast, inexpensive and efficient technique [2] for hadron identification. Its implementation at HERMES is possible because of a) the presence of two scintillator counter walls H1 and H2 in the HERMES spectrometer, and b) the fine time structure of the HERA electron beam (with bunch lengths of 27 ps and time between bunches of 96 ns), which allows particles from different bunches to stay completely separated in time.

2 Counter Design

HERMES is a forward spectrometer with a large dipole magnet, a set of tracking detectors, and particle identification (PID) detectors consisting of a Čerenkov detector, a Transition Radiation Detector (TRD), a preshower detector and a calorimeter [1]. In 1998 the threshold-Čerenkov counter was upgraded to a Ring Imaging Čerenkov (RICH) detector [3]. A scintillator hodoscope (H1) and a Pb-scintillator

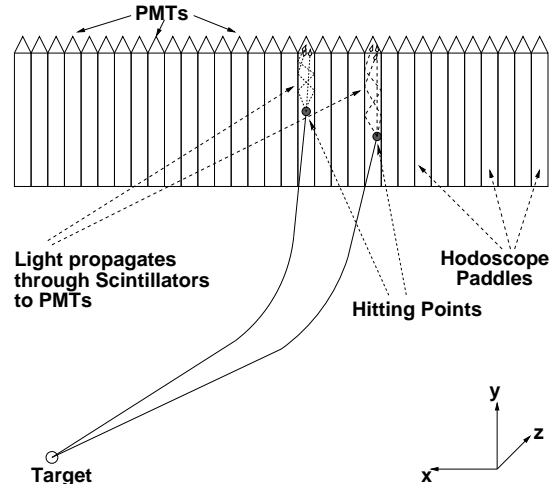


Fig. 1. Schematic view of particle tracks and hodoscope paddles (upper part).

preshower counter (H2) (Fig. 1) provide trigger signals and particle identification information. Both counters are composed of vertical scintillator modules (42 each in the upper and lower detectors), which are 1 cm thick and 9.3 cm x 91 cm in area. The material for the modules is BC-412 from Bicron Co., a fast scintillator with large attenuation length (300-400 cm for scintillation light). The scintillation light is detected by 5.2 cm diameter Thorn EMI 9954 photomultiplier tubes coupled via a light guide to the outer end of each scintillator (away from the beam plane). The modules are staggered to provide maximum efficiency with 2-3 mm of overlap between each unit. Each hodoscope photomultiplier (PMT) signal is passively split with one output going to a LeCroy 1881M ADC and the other going to a LeCroy 3420 Constant Fraction Discriminator (CFD). The individual CFD outputs are fed to LeCroy 1875A time to digital converters (TDC), which measure the time-of-flight using the HERA-clock as a reference signal. This signal corresponds to the moment when the HERA bunch crosses the center of the target. When some interesting event configu-

ration is recognized by the HERMES trigger logic, the HERA-clock signal is enabled to start the TDC modules in common-start mode, with the STOP signals coming from each scintillator. The time base for the TDC is 50 ps/channel.

3 Calibration procedure

The calibration procedure is based on the fact that electrons above 10 MeV are moving at essentially the speed of light. Any measured deviations from this must be artifacts of the experiment that should be corrected.

In Fig. 2 the time distribution for electrons over the paddles is shown for part of one detector. The electron sample is selected by a combination of cuts on TRD, Čerenkov, Preshower and Calorimeter. The

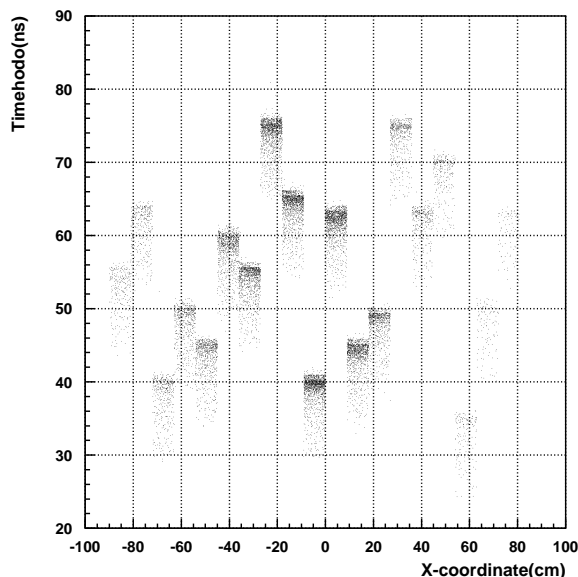


Fig. 2. Non- equalized time dependence over X-coordinate

time distribution is spread within each paddle as well as between paddles. The differences between the paddles (due to different cable lengths, etc) were removed by setting

the average speed of the electrons to the speed of light for each paddle individually. A single-counter time response is described by

$$t = t_{pf} + t_{lf} + t_0 \quad (1)$$

where t_{pf} is the particle time-of-flight from the interaction point to the scintillator plane, t_{lf} is the time needed for the light created in the scintillator to reach the PMT, t_0 is the constant time offset specific to each paddle, arising from the PMT response time, cable delays, TDC calibration intercept, etc. The path length l_H of each track to hodoscope H was calculated using the reconstructed track parameters, along one straight line segment from the interaction point in the target to the mid-plane of the spectrometer magnet, and continuing along another straight line from there to the plane of the hodoscope H. This approximation is adequate because the magnet bend angle is less than $\pi/20$. The calibration for each paddle n of hodoscope H was done with electron tracks by fitting the y -distribution of $1/v = t/l_H$ shown in Fig. 3 to the known value of $1/c$ using a fourth-order correction polynomial $F_n(y)$:

$$F_n(y) = 1/c - t/l_H.$$

The constant term in the polynomial incorporates t_0 in Eq. 1 for each paddle. A similar method has been used in [4] where a more detailed explanation for each coefficient of the polynomial is given. Occasional shifts in the HERA-clock signal derived from the electron beam accelerator system, shown in Fig. 4, were compensated by re-fitting the constant term for each run of approximately 10 minutes. The final corrected distribution of $1/v_e = t/l_H + F_n(y)$ for electrons is shown in Fig. 5. The resolution extracted from a Gaussian fit corresponds to $\sigma=0.49$ ns.

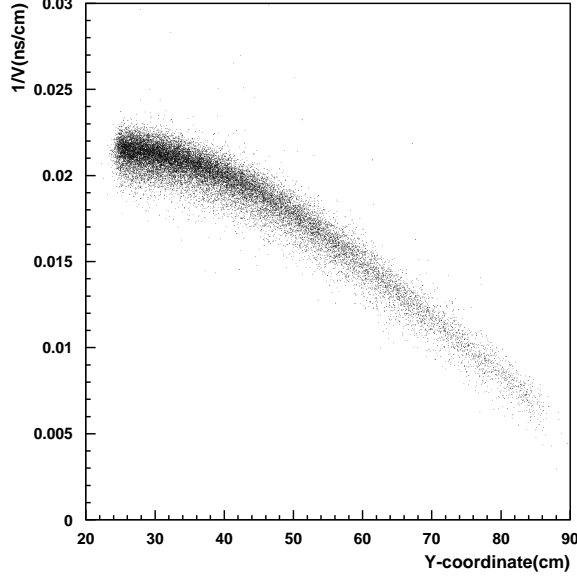


Fig. 3. $1/v_e$ non-equalized dependence on the Y-coordinate for electrons (single paddle).

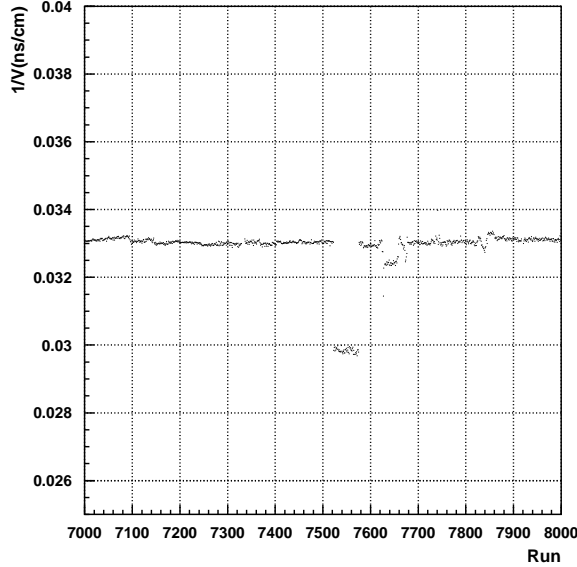


Fig. 4. Y corrected $1/v_e$ dependence on run numbers (for electrons).

4 Hadron Identification via Time-of-Flight

From the relativistic momentum of the particle

$$p = m \cdot \beta / \sqrt{1 - \beta^2}, \quad (2)$$

the mass m is extracted using the speed

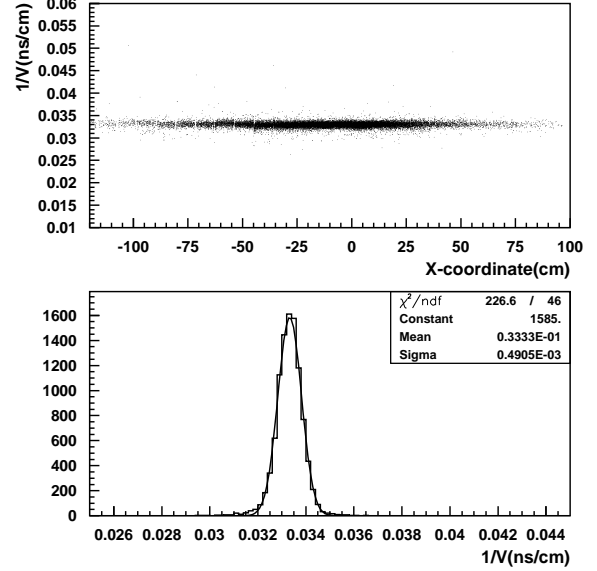


Fig. 5. $1/v_e$ for electrons in hodoscope H1 (equalized and run-corrected).

$\beta = v/c$ obtained through the hodoscope timing:

$$m^2 = p^2 \left(\frac{1}{\beta^2} - 1 \right). \quad (3)$$

The squared mass of the particle was chosen as the parameter for the identification. To check the algorithm and calibration, the proton and kaon squared masses have been extracted giving values of $m_p^2 = 0.88$ $(\text{GeV}/c^2)^2$ and $m_K^2 = 0.25$ $(\text{GeV}/c^2)^2$, respectively, which agrees well with the expected values (Fig. 6). At momenta below 2 GeV/c the kaon flux is two orders of magnitude smaller than the pion flux, so that no separation is possible via TOF for momenta above 1.5 GeV/c. Therefore in the momentum range $1.5 < p < 2.0$ GeV/c, kaons are included in the pion spectrum as a negligible contamination ($< 1\%$). At higher momenta, a RICH detector takes over.

Fig. 7 shows the squared hadron mass distribution for the momentum region $1.5 < p < 2.0$ GeV/c. The good separation between protons and pions is clearly visible. Using TOF information from only one detector (e.g. hodoscope H1), the upper

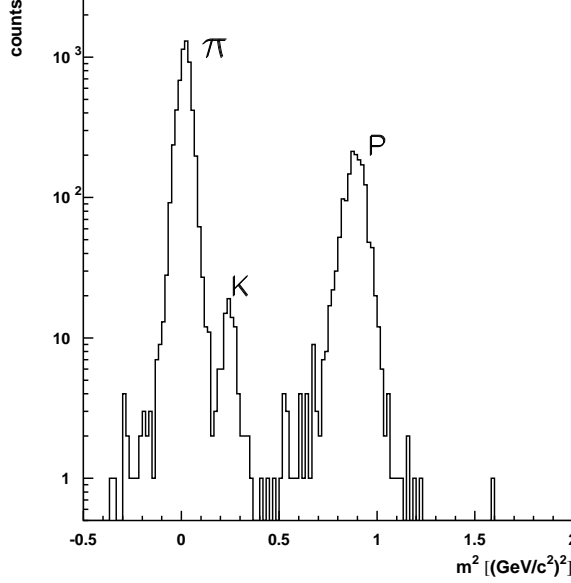


Fig. 6. m^2 distribution for hodoscope H1 upper detector), $0.6 < p < 1.1$ GeV/c. Log scale is chosen due to significant difference between different particles fluxes.

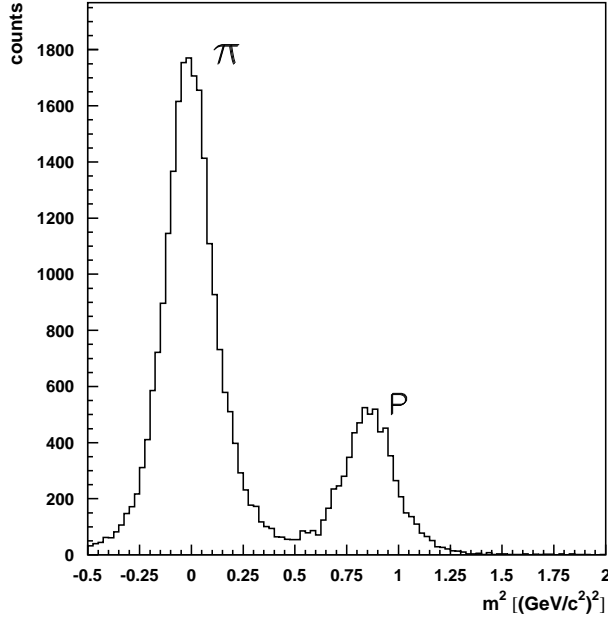


Fig. 7. m^2 distribution for hodoscope H1 (upper detector), $1.5 < p < 2.0$ GeV/c

bound for the separation is about 2.4 GeV/c. The availability of two independent detectors H1 and H2 suggests the use of two-dimensional distributions, as shown in Fig. 8. Independent constraints on the TOF values from both hodoscopes is the best

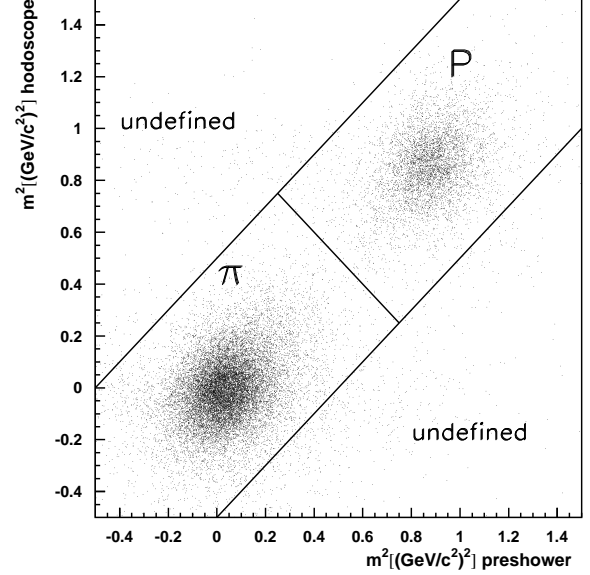


Fig. 8. Two-dimensional distribution of squared mass from Hodoscope(H1) and Preshower(H2) for the momentum region $1.5 < P < 2.0$ GeV/c.

strategy to minimize the contamination. However, this is not the best way to maximize the efficiency while maintaining a low contamination. In the case of two detectors a linear 'valley cut' in the plane of the two detector responses gives an improvement [5]. It is possible to apply the combined constraint on the sum $m_{H1}^2 + m_{H2}^2$. This evaluation provides an improvement in the separation between protons and pions - especially for higher momenta - and therefore extends the momentum region for hadron identification with high efficiency and low contamination. The identification of kaons is limited to $p < 1.5$ GeV/c, due to the very low kaon flux (see Fig. 6). The comparison of the pion contamination in the proton sample for individual constraints on the two hodoscopes with that for the combined constraint is presented in Fig. 9.

The most important parameters for particle identification are the efficiency for identification of certain particle types and the contamination from other types. Fig. 10

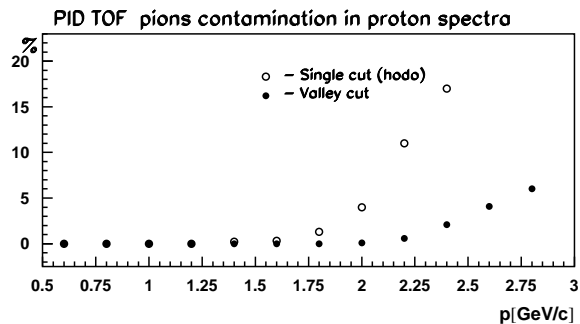


Fig. 9. Pion contamination in the proton sample for the cases of individual constraints on one of the two hodoscopes with that for the combined constraint.

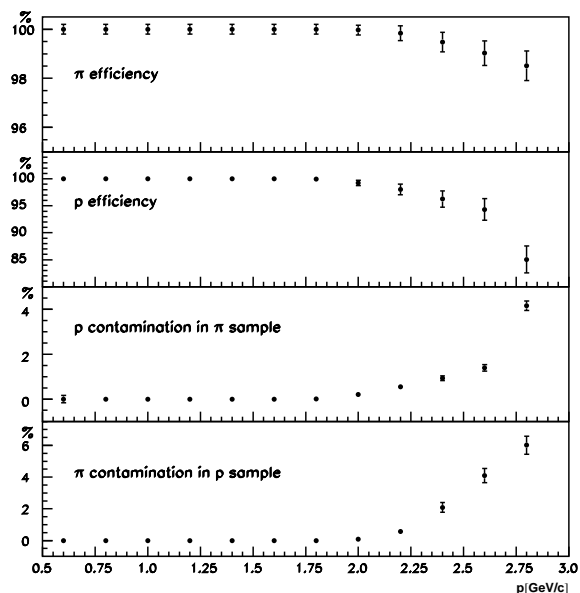


Fig. 10. Proton and pion identification efficiency and contamination vs momenta for the valley cut.

presents both parameters for proton and pion identification. The valley cut allows identification of protons and pions up to 2.9 GeV/c. The resulting pion sample has an efficiency above 98% and less than 4% proton contamination, while the protons have an efficiency of more than 85% and less than 6% pion contamination in the highest momentum bin. All analysis was done using semi-inclusive data samples from the year 1997 on polarized hydrogen target.

5 Conclusion

The TOF method, as presented in this paper, allows an extension of the momentum range for hadron identification in HERMES towards lower momenta. The application of this method provides more statistics for hadrons detected within the HERMES acceptance and extends the minimum value of $z = \frac{E_h}{\nu}$, where E_h is the hadron energy and ν is the virtual photon energy.

6 Acknowledgements

We gratefully acknowledge the DESY management for its support and the DESY staff and the staffs of the collaborating institutions for their strong and enthusiastic support.

References

- [1] HERMES Collaboration, K. Ackerstaff *et al*, Nucl.Instr. and Meth.**A417** (1998) 230.
- [2] W.B. Atwood, SLAC-Pub-2620, 1980.
- [3] N. Akopov *et al.*, The HERMES Dual-Radiator Ring Imaging Čerenkov Detector, NIM A479 (2002) 511-530.
- [4] J.N. Synodinos, Ph.D. Thesis, SLAC-R-0470, 1995.
- [5] R. Kaiser, Ph.D.Thesis, HERMES 97-017, 1997.